Dual Polarization and Bi-Directional Silicon-Photonic Optical Phased Array With Large Scanning Range

Shi Zhao, Jingye Chen, and Yaocheng Shi, *Member, IEEE*

***Abstract*—We propose a large scanning range silicon optical phased array (OPA), which is polarization multiplexed and bi-directional with only one waveguide grating antenna array. Mach-Zehnder interferometers (MZIs) and polarization splitter-rotator (PSR) are utilized to select the polarization states and propagation directions of the input light to the waveguide grating emitter array. By optimizing the parameters of the waveguide grating, the longitudinal far-field steering range is increased by four times compared to that of the conventional ones among the same wavelength range. The simulation results show that the 54.5° longitudinal scanning range could be realized with the tuning wavelength ranging from 1500 nm to 1600 nm. The high wavelength tuning efficiency is up to 0.545 °/nm. The beam steering range in the lateral direction is 77.8° via phase tuning.**

***Index Terms*—Optical phased array, silicon-on-insulator, silicon photonics.**

I. Introduction

THE silicon-on-insulator (SOI) is an attractive platform for high-density integration due to its complementary metal oxide semiconductor (CMOS) compatibility [1]. The integrated optical phased array (OPA) based on SOI platform has the advantages of low cost, easy integration and high stability, which could be a significant component in light detection and ranging (LiDAR) system [2]. In order to obtain two-dimensional (2D) beam steering, one way is to use phase tuning in both dimension [3], [4]. However, each phase element should be independent, which makes the phase control system and waveguide arrangement complicated. Furthermore, the large spacing between the array emitters severely limits the beam steering angle. Another commonly used method is to introduce wavelength tuning using waveguide grating into the one-dimensional (1D) OPA [5]–[11], thus 2D beam steering is realized by combining wavelength and phase tuning. However, the wavelength tuning range is usually ∼100 nm, corresponding to the steering angle ∼14° [8], [9], limited by the working bandwidth of the light source and the key components such as the power splitters. Four OPAs with different output grating emitter arrays are integrated in a single chip to increase the wavelength tuning efficiency [11]. By using the optical switches to select different emission gratings, the total scanning angle reaches 28.5° with wavelength ranging from 1520 nm to 1570 nm. Although such multi-lines OPA can overcome the limitation of steering angle caused by limited bandwidth, the complexity of the chip is increased dramatically.

By introducing dual polarization, the deflection angle can be approximately doubled. Due to the significant birefringence, the SOI-based waveguide is usually polarization dependent [12]. As shown in the reference [10], a feasible solution is to combine polarization control devices and OPA to realize large range continuous scanning by optimizing the parameters of waveguide grating so that the steering angle for the fundamental transverse electric mode (TE_0) is adjacent to that of the fundamental transverse magnetic mode (TM_0). In this paper, we propose a polarization multiplexed OPA with a bi-directional shared grating emitter array to further improve the longitudinal steering angle and wavelength tuning efficiency. Two identical OPAs are placed on each side of the emitter array. Two-stage MZIs are used to select the directions and polarization states of the light injected into the emitter array. By optimizing the waveguide width and the grating period, dual polarization multiplexed and bi-directional OPAs could complement blind area in the scanning range. Based on such design, the total longitudinal scanning angle reaches 54.5° with the wavelength scanning range from 1500 nm to 1600 nm. The lateral steering range is ∼77.8° by using phase tuning with a waveguide interval 1.2 μm.

II. Design and Analysis

The schematic diagram of the proposed dual polarization multiplexed OPA is shown in Fig. 1(a), which consists of two Mach-Zehnder interferometers (MZIs), polarization splitter-rotator (PSR) and two OPAs. Fig. 1(b) shows the cross section view of the optical waveguide. The SOI platform with a 340 nm-thick core silicon layer and 2 μm-thick buried oxide layer is considered in this work. The waveguide width W_{wg} is designed to be 400 nm to ensure the fundamental-mode propagation. The TE polarized light is injected from the input grating. The first stage MZI (MZI I) switch is used to determine the light propagation direction. When it is on, the light injects into emission grating from the left

Manuscript received January 10, 2022; revised February 18, 2022; accepted February 19, 2022. Date of publication February 23, 2022; date of current version April 6, 2022. This work was supported by the National Natural Science Foundation of China under Grants 62105286 and 61922070. *(Corresponding authors: Jingye Chen and Yaocheng Shi.)*

The authors are with the State Key Laboratory for Modern Optical Instrumentation, Center for Optical and Electromagnetic Research, College of Optical Science and Engineering, Ningbo Research Institute, International Research Center for Advanced Photonics, Zhejiang University, Hangzhou 310058, China (e-mail: zhaoshi@zju.edu.cn; jingyechen@zju.edu.cn; yaocheng@zju.edu.cn).

Digital Object Identifier 10.1109/JPHOT.2022.3153507

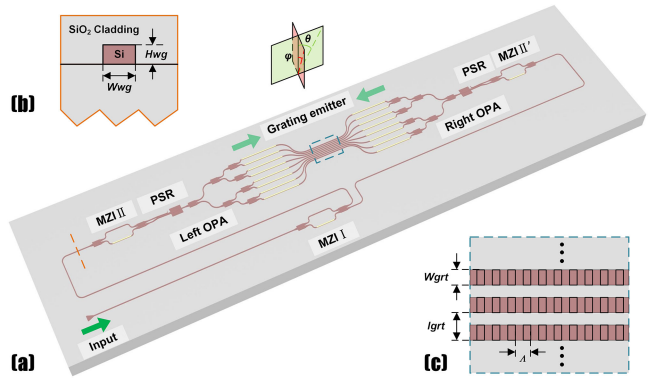

Fig. 1. Schematic diagram of the proposed bi-directional dual polarization multiplexed OPA. (a) 3D view; (b) Cross section view of waveguide; (c) Top view of the waveguide grating emitter.

side, otherwise from the right side. The second stage MZI (MZI II and II') together with the reversed PSR [13] constitutes the polarization selector. The switch state of the MZI could determine which port light enters the reversed PSR. When the light is from the upper port, the TE polarization light will be converted into TM polarization light after passing through the PSR. When the light is from the lower port, the polarization state will remain unchanged. Therefore, both the propagation direction and the polarization state can be controlled by the switch states of the two-stage MZIs. The top view of the waveguide grating emitter is shown in Fig. 1(c). The left-hand side is the negative angle of θ, and the right-hand side covers the positive angle (shown in Fig. 1(a)). The longitudinal beam steering angle of the grating emitter is determined by the following equation:

$$\sin\theta = \frac{\Lambda n_{eff} - \lambda_0}{n_{bg}\Lambda} \tag{1}$$

Where Λ is the grating period, n_{eff} is the effective index of the guiding mode. n_{bg} is the background index. Here the background is air, thus, $n_{bg} = 1$. λ_0 is the wavelength of the incident light. According to (1), the longitudinal beam steering angle is determined by the grating parameters and operating wavelength. Once the grating structure parameters are determined, the longitudinal beam steering in a certain range can be realized by adjusting the working wavelength. Fig. 2(a) shows calculated effective index of the TE_0 mode and TM_0 mode with different waveguide widths from 0.4 μm to 1.5 μm. The difference of n_{eff} between the TE_0 and TM_0 modes increases gradually with the waveguide width and tends to be stable. Because of the large polarization dispersion of waveguide for the silicon waveguide, the deviation of the far-field beam scanning angle for different polarization states is large, and the far-field continuous scanning cannot be realized by just adjusting the wavelength. Thus, conventional OPA operates in a specific polarization state only with an angular deflection of about $\sim$14° in $\sim$100 nm wavelength range [8], [9]. Here, we make reasonable use of waveguide polarization dispersion to achieve large longitudinal scanning range. Two identical OPAs are placed on either side of the grating emitter. When the light is incident from the right

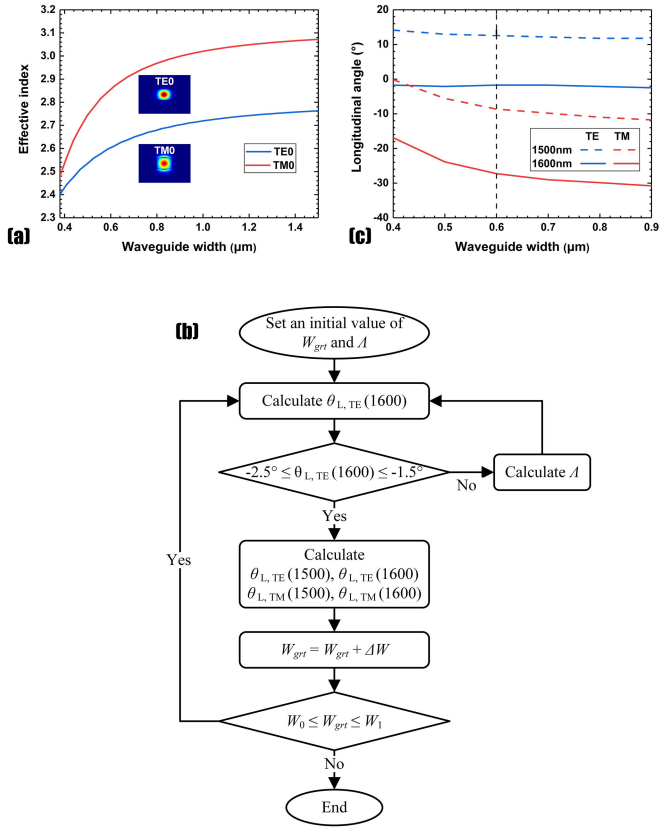

Fig. 2. (a) The effective index of the TE0 mode and TM0 mode with different waveguide widths from 0.4 μm to 1.5 μm. (b) The flow chart of the longitudinal beam angle optimization process. (c) The longitudinal beam angle for two polarization states with different waveguide width from 0.4 μm to 0.9 μm.

OPA, the far field angle is symmetric with that of the left OPA about the $\theta = 0°$ plant under the same condition. Therefore, the longitudinal beam steering angle for the right OPA is determined by the following equation:

$$\sin_{\mathrm{R}}(\theta) = -\frac{\Lambda n_{eff} - \lambda_0}{n_{bg}\Lambda} \tag{2}$$

In order to achieve large scanning range without blind areas, the far-field steering angle of OPAs should satisfy the following conditions:

$$\theta_{\mathrm{L,TE}}\,(1600) \le \theta_{\mathrm{R,TE}}\,(1600) \tag{3}$$

$$\theta_{\mathrm{L,TE}}\,(1500) \ge \theta_{\mathrm{R,TM}}\,(1500) \tag{4}$$

Where $\theta_{\mathrm{L,\,TE}}\,(1600)$ refers to longitudinal beam steering angle of the left OPA with wavelength $\lambda_0 = 1600$ nm. The others parameters are similarly named. The (3) and (4) could ensure that the far-field scanning range of TE polarization of one OPA can completely cover the interval between the far-field scanning range of two polarization states of the other OPA.

The device is simulated and optimized using the three-dimensional finite-difference time-domain (3D-FDTD) method. The etching depth is chosen to be $H_{\mathrm{etc}} = 70$ nm. The duty cycle is 0.5. To satisfy (3), we fix $\theta_{\mathrm{L,\,TE}}\,(1600)$ around $-2°$. A 4° of far-field overlap around 0° could provide large fabrication tolerance

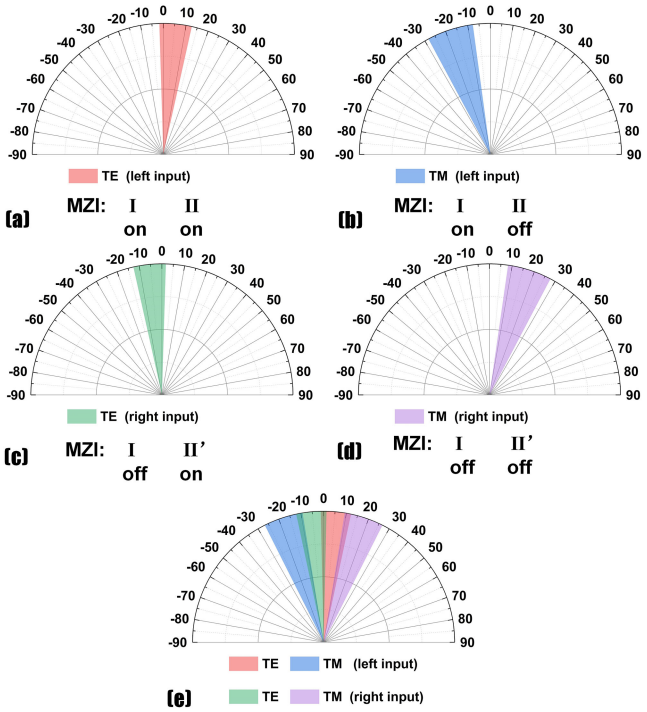

Fig. 3. (a)–(d) The scanning range for different states of MZIs. (e) The total longitudinal scanning range of the proposed polarization multiplexing OPA.

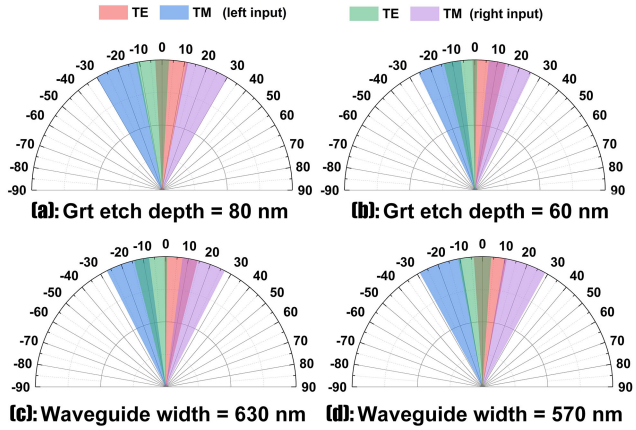

Fig. 4. (a)–(d) Calculated longitudinal scanning range with deviated waveguide width or etching depth.

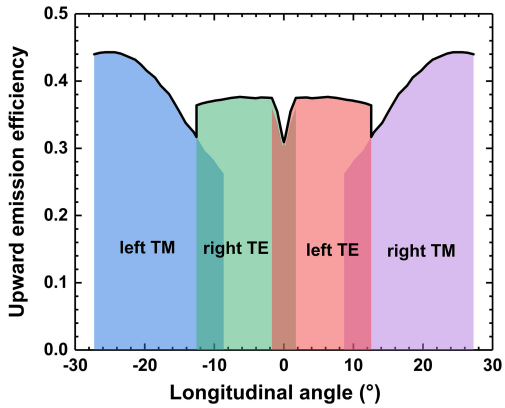

Fig. 5. The simulated upward emission efficiency of emission grating.

for the emission grating without wasting much steering range. Firstly, the n_{eff} of TE polarization corresponding to the grating parameters can be calculated as $n_{eff} = (\sin\theta \cdot n_{bg} \cdot \Lambda + \lambda_0)/\Lambda$ according to (1). Then the calculated n_{eff} is returned to (1), and the period to be solved can be calculated as following $\Lambda = \lambda_0/(n_{eff} - \sin(-2°) \cdot n_{bg})$. Finally, the longitudinal scanning range of two polarization states for left OPA with $\theta_{\mathrm{L,\ TE}}$ (1600) fixing around $-2°$ is calculated as shown in Fig. 2(c). Fig. 2(b) shows the optimization process in detail. The waveguide width W_{grt} varies from $W_0 = 0.4\ \mu$m to $W_1 = 0.9\ \mu$m with a step of $\Delta W = 0.1\ \mu$m. In Fig. 2(c), the dashed and solid lines represent the variation of θ with the waveguide width W_{grt} when the operating wavelength is 1500 nm and 1600 nm. The blue and red lines refer to the two polarization states. The interval between the solid and dashed lines of the same color represents the range of the longitudinal beam steering angle that can be covered, and the interval between the solid line and dotted line of different colors represents the blind area of scanning range. As the waveguide width increases, the distance between the corresponding deflection ranges of the two polarization states is gradually separated. To satisfy (4), the waveguide width is chosen to be $W_{grt} = 0.6\ \mu$m considering the trade-off between the scanning range and the fabrication feasibility. According to (1), the grating period is calculated to be $\Lambda = 574$ nm. The transmission of four different OPA states is represented by blue, green, pink and purple respectively. As shown in Fig. 3(a)–(d), the scanning range for different on/off states of MZIs are $(-1.7°, 12.6°)$, $(-27.3°, -8.7°)$, $(-12.6°, 1.7°)$ and $(8.7°, 27.3°)$ respectively. Combining the four states, the proposed dual polarization multiplexed and bi-directional OPA achieves free-space beam steering in longitudinal dimension with 54.5° field of view.

However, the variation of waveguide width and etching depth will affect the effective refractive index of the guide mode and change the far-field beam steering angle. In order to overcome the effect of the fabrication error, we reserve overlap region of 4° at the three splices, which are located at $-10.5°$, 0°, and 10.5°, for the designed grating emitter. The total longitudinal scanning range for the emission grating are calculated with deviated waveguide width or etching depth, as shown in Fig. 4(a)–(d). By changing the grating parameters, the proposed OPA could works normally with no blind area appearing between the maximum and minimum angles of the scanning range. Large scanning range of $> 50.3°$ can still be achieved with $\triangle W_{grt} = \pm 30$ nm or $H_{etc} = \pm 10$ nm.

Fig. 5 shows the upward emission efficiency (UEE) of the grating emitter with different polarizations and incident directions. In order to obtain higher upward efficiency, the OPA state with higher efficiency is selected as the UEE of the system in the overlap region. Therefore, the UEE of the proposed OPA is greater than 0.3 with the longitudinal steering angle ranging from $-27.3°$ to 27.3°, which is shown in Fig. 5.

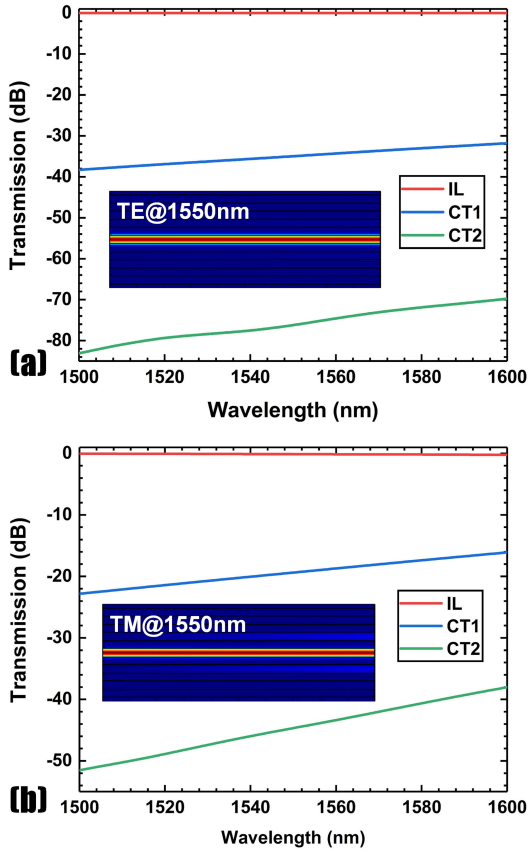

Fig. 6. The crosstalk of adjacent and sub-adjacent waveguides for TE_0 (a) and TM_0 (b) With the waveguides spacing of 1.2 μm and length of 100 μm. The inserted figures are the light propagation profiles at waveguide of 1550 nm.

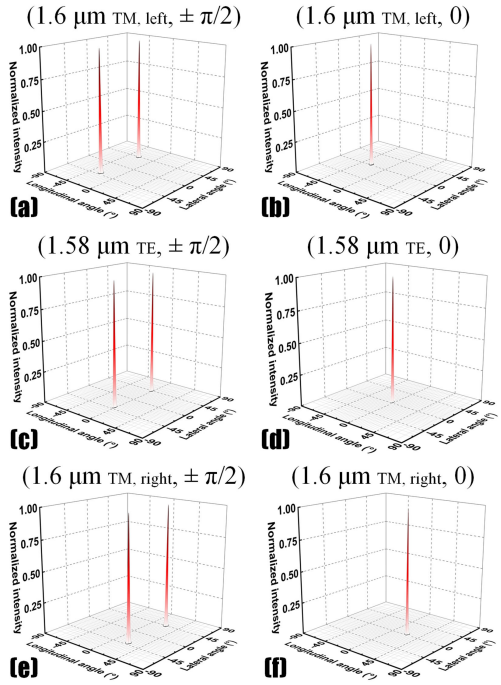

Fig. 7. The far field distribution for the proposed OPA with different wavelength and phase shift.

TABLE I
COMPARISON PERFORMANCES OF THE OPAS IN THE DIRECTION OF WAVELENGTH TUNING*

Ref.	Method	Number of emitter array	Longitudinal scanning range (°)	Wavelength tuning efficiency (°/nm)
[3]	Conventional grating	1	14.1	0.141
[10]	Polarization multiplexing	1	28.2	0.282
[11]	Multi-Lines	4	28.94	0.579
[19]	Polarization multiplexing	2	51	0.46
Our work	Polarization multiplexing and bi-direction	1	54.5	0.545

*All the data in table are simulation results.

In the lateral direction, the beam steering is achieved by changing the phase difference between adjacent waveguides. The narrower the waveguide spacing is, the larger the field of view without grating lobes can be obtained [14]. When the waveguides are spaced at half of the operating wavelength, there is only one main lobe at $\pm$ 90° field of view [14], [15]. However, the crosstalk between waveguides increases when the waveguides get closer [16]. Considering the tradeoff between scanning range and crosstalk, the waveguide interval is chosen to be $l_{grt} = 1.2$ μm. The waveguide grating emitter length is chosen to be 100 μm to ensure that most of the light could be radiated upward through the emitter grating. Here, we denote the Insertion loss (IL) and crosstalk (CT) as:

$$IL = 10\log_{10} T_{\mathrm{wg0}} \tag{5}$$

$$CT1(2) = 10\log_{10} T_{\mathrm{wg1(2)}} \tag{6}$$

Where the T_{wg0} is the transmission of the incident waveguide, and T_{wg1} (T_{wg2}) is the transmission of the adjacent and sub-adjacent waveguides. As shown in Fig. 6(a), one can find that the crosstalk of adjacent and sub-adjacent waveguides for TE_0 are below $-$ 30 dB and $-$ 70 dB with wavelength ranging from 1500 nm to 1600 nm. For the conventional directional coupler, the coupling strength for TM polarization is much higher than that of TE polarization [17]. Hence, the crosstalk of TM_0 is higher than TE_0. However, the crosstalk can still remain below $-$ 16 dB, as shown in Fig. 6(b).

The whole grating emitter is also calculated by using 3D-FDTD. The number of emitter array element is set to be 16. In lateral direction, the large separation, greater than half a wavelength, will cause unwanted high order grating lobes in the far field [15]. When the phase difference between the adjacent waveguides is $\pm$ π/2, the two grating lobes are axial symmetry. Fig. 7 shows the simulated far-field distribution for the proposed OPA with the wavelength and phase shift at certain values, such as (1.6 μm $_{\mathrm{TM,\ left}}$, $\pm$ π/2), (1.6 μm $_{\mathrm{TM,\ left}}$, 0), (1.58 μm $_{\mathrm{TE}}$, $\pm$ π/2), (1.58 μm $_{\mathrm{TE}}$, 0), (1.6 μm $_{\mathrm{TM,\ right}}$, $\pm$ π/2) and (1.6 μm $_{\mathrm{TM,\ right}}$, 0), respectively. The calculated result indicates that the scanning range is up to 54.5° $\times$ 77.8°. The

full width at half maximum (FWHM) of the longitudinal and lateral beam are calculated to be ~ 2 ° and ~ 3.6 °, which could be further improved by reducing grating strength [18] and increasing the number of waveguides.

III. Conclusion

In conclusion, we propose and design a dual polarization multiplexed and bi-directional silicon OPA with a shared emitter array. Two identical OPAs connected by MZI switches are placed on either side of the emitter array. The two-stage MZI is used to select the propagation direction and polarization state of light propagated in the emitter. The beam of the two OPAs with only one emitter array can be steered without blind area in the field of view and achieve a large scanning range. From the simulation results, one can find that the total scanning range of $54.5° \times 77.8°$ can be achieved by combining wavelength tuning and phase tuning. We also summarize the performances of the reported state-of-the-art OPA in Table I. The wavelength tuning efficiency can be improved by increasing the number of emitters [11], [19] or introducing polarization multiplexing [10], [19]. To the best of our knowledge, the proposed dual polarization and bi-directional OPA could obtain the higher wavelength tuning efficiency of about 0.545 °/nm with only one waveguide grating antenna array. The FWHM for the longitudinal and lateral direction are calculated to be $\sim 2°$ and $\sim 3.6°$. The emission gratings can be fabricated friendly with a large fabrication tolerance. We believe the proposed OPA could be further improved in beam steering range and resolution, making it promising to be applied in the optical communication and LiDAR.

References

[1] J. Chen, Y. Sun, S. Wei, X. Han, and Y. Shi, "Optical phased array based on silicon waveguides with non-uniform widths," in *Proc. 23rd Opto-Electron. Commun. Conf.*, 2018, pp. 1–2.

[2] M. J. R. Heck, "Highly integrated optical phased arrays: Photonic integrated circuits for optical beam shaping and beam steering," *Nanophotonics*, vol. 6, no. 1, pp. 93–107, 2017.

[3] K. V. Acoleyen, W. Bogaerts, J. Jágerská, N. L. Thomas, R. Houdré, and R. Baets, "Off-chip beam steering with a one-dimensional optical phased array on silicon-on-insulator," *Opt. Lett.*, vol. 34, no. 9, pp. 1477–1479, May 2009.

[4] J. Sun, E. Timurdogan, A. Yaacobi, E. S. Hosseini, and M. R. Watts, "Large-scale nanophotonic phased array," *Nature,* vol. 493, no. 7431, pp. 195–199, Jan. 2013.

[5] D. N. Hutchison *et al.*, "High-resolution aliasing-free optical beam steering," *Optica,* vol. 3, no. 8, pp. 887–890, Aug. 2016.

[6] R. Fatemi, A. Khachaturian, and A. Hajimiri, "A nonuniform sparse 2-D large-FOV optical phased array with a low-power PWM drive," *IEEE J. Solid-State Circuit*, vol. 54, no. 5, pp. 1200–1215, May 2019.

[7] S. A. Miller *et al.*, "Large-scale optical phased array using a low-power multi-pass silicon photonic platform," *Optica,* vol. 7, no. 1, pp. 3–6, Jan. 2020.

[8] J. K. Doylend, M. J. R. Heck, J. T. Bovington, J. D. Peters, L. A. Coldren, and J. E. Bowers, "Two-dimensional free-space beam steering with an optical phased array on silicon-on-insulator," *Opt. Exp.,* vol. 19, no. 22, pp. 21595–21604, Oct. 2011.

[9] P. Wang *et al.*, "Design and fabrication of a SiN-Si dua-layer optical phased array chip," *Photon. Res.,* vol. 8, no. 6, pp. 912–919, Jun. 2020.

[10] X. Yan, J. Chen, D. Dai, and Y. Shi, "Polarization multiplexing silicon-photonic optical phased array for 2D wide-angle optical beam steering," *IEEE Photon. J.,* vol. 13, no. 2, Apr. 2021, Art. no. 6600506.

[11] L.-X. Zhang *et al.*, "Large-scale integrated multi-lines optical phased array chip," *IEEE Photon. J.,* vol. 12, no. 4, Aug. 2020, Art. no. 6601208.

[12] H. Xu and Y. Shi, "Subwavelength-grating-assisted silicon polarization rotator covering all optical communication bands," *Opt. Exp.,* vol. 27, no. 4, pp. 5588–5597, Feb. 2019.

[13] D. Dai, J. Bauters, and J. E. Bowers, "Passive technologies for future large-scale photonic integrated circuits on silicon: Polarization handling, light non-reciprocity and loss reduction," *Light-Sci. Appl.,* vol. 1, no. 3, pp. e1–e1, 2012.

[14] X. Yi, H. Zeng, S. Gao, and C. Qiu, "Design of an ultra-compact low-crosstalk sinusoidal silicon waveguide array for optical phased array," *Opt. Exp.*, vol. 28, no. 25, pp. 37505–37513, Dec. 2020.

[15] C. T. Phare, C. S. Min, S. A. Miller, B. Stern, and M. Lipson, "Silicon optical phased array with high-efficiency beam formation over 180 degree field of view," in *Conf. Lasers Electro-Optics (CLEO)*, 2018, Paper SM3I.2.

[16] Y. Zhang *et al.*, "Sub-wavelength-pitch silicon-photonic optical phased array for large field-of-regard coherent optical beam steering," *Opt. Exp.*, vol. 27, no. 3, pp. 1929–1940, Feb. 2019.

[17] H. Xu and Y. Shi, "Ultra-compact polarization-independent directional couplers utilizing a subwavelength structure," *Opt. Lett.,* vol. 42, no. 24, pp. 5202–5205, Dec. 2017.

[18] W. Xie *et al.*, "Heterogeneous silicon photonics sensing for autonomous cars," *Opt. Express*, vol. 27, no. 3, pp. 3642–3663, Feb. 2019.

[19] X. Han *et al.*, "Solid-state photonics-based lidar with large beam-steering angle by seamlessly merging two orthogonally polarized beams," *IEEE J. Sel. Topics Quantum Electron.,* vol. 27, no. 1, Jan./Feb. 2021, Art. no. 8300608.